Supplemental Material for
"Effective $J=1/2$ insulating state in Ruddlesden-Popper iridates: An LDA+DMFT study"

Hongbin Zhang,[*] Kristjan Haule, and David Vanderbilt

Department of Physics and Astronomy, Rutgers University, Piscataway, USA

I.   COMPUTATIONAL DETAILS

Our all-electron DFT+DMFT implementation[1] extremizes the following functional[2]

$$\Gamma[\rho, V_{KS}, G_{loc}, \Sigma, V_{dc}, n_d] = -\operatorname{Tr}\ln\left((i\omega + \mu + \nabla^2 - V_{KS})\delta(\mathbf{r}-\mathbf{r}') - \sum_{\tau LL'} P(\mathbf{rr}',\tau LL')(\Sigma - V_{dc})_{L'L}\right) \tag{1}$$

$$-\int [V_{KS} - V_{ext}]\rho d^3 r - \operatorname{Tr}(\Sigma G_{loc}) + \operatorname{Tr}(V_{dc} n_d) + \Phi_H[\rho] + \Phi_{xc}[\rho] + \Phi_{\mathrm{DMFT}}[G_{loc}] - \Phi_{dc}[n_d]$$

of three pairs of conjugate variables. Imposing stationarity leads to

$$\frac{\delta\Gamma}{\delta V_{KS}} = 0 \; : \; \operatorname{Tr}_\omega(G(\mathbf{rr}')\delta(\mathbf{r}-\mathbf{r}')) - \rho(\mathbf{r}) = 0 \tag{2}$$

$$\frac{\delta\Gamma}{\delta\rho} = 0 \; : \; -(V_{KS} - V_{ext}) + \frac{\delta[\Phi_H + \Phi_{xc}]}{\delta\rho} = 0 \tag{3}$$

$$\frac{\delta\Gamma}{\delta G_{loc}} = 0 \; : \; -\Sigma + \frac{\delta\Phi^{\mathrm{DMFT}}[G_{loc}]}{\delta G_{loc}} = 0 \tag{4}$$

$$\frac{\delta\Gamma}{\delta\Sigma} = 0 \; : \; \operatorname{Tr}_{\mathbf{r}}(P(\mathbf{rr}',\tau LL')G) - G_{loc} = 0 \tag{5}$$

$$\frac{\delta\Gamma}{\delta V_{dc}} = 0 \; : \; -\operatorname{Tr}_{\omega\mathbf{r}}(P(\mathbf{rr}',\tau LL')G) + n_d = 0 \tag{6}$$

$$\frac{\delta\Gamma}{\delta n_d} = 0 \; : \; V_{dc} - \frac{\delta\Phi_{dc}}{\delta n_d} = 0 \tag{7}$$

where $\operatorname{Tr}_\omega = T\sum_{i\omega_n}$ and $\operatorname{Tr}_{\mathbf{r}} = \int d^3 r d^3 r'$. At the saddle-point ρ and V_{KS} are the electronic charge density and the Kohn-Sham potential, G_{loc} and Σ are the local Green's function and DMFT self-energy, V_{dc} is the double-counting potential, and n_d is the occupancy of the correlated orbital, $\Phi_H[\rho]$ and $\Phi_{xc}[\rho]$ are the Hartree and the exchange-correlation energy functionals, and $\Phi_{\mathrm{DMFT}}[G_{loc}]$ is the sum of all skeleton diagrams constructed from G_{loc} and local Coulomb repulsion $\hat{U}$. This summation is carried out by the impurity solver. The local Coulomb repulsion $\hat{U}$ is parametrized with Slater parametrization. The impurity model is solved by the continuous-time quantum Monte Carlo method.[3,4]

V_{ext} is the external potential, containing the material specific information. $P(\mathbf{rr}',\tau LL')$ is the projector to the local correlated orbital at atom τ with angular momentum indices L, L'. We use the projector $P^2(\mathbf{rr}',\tau LL')$

introduced in Ref. 1 with an energy window of $\approx 20\,eV$ around the Fermi level. For maximal locality of correlated states, this projector is implemented in real space. The iridium t_{2g} states are treated dynamically, while the rest of the valence states in the interval of $\approx 20\,eV$ are treated in a mean-field way.

For the double-counting correction, the method explained in Ref. 1 is used, where $\Phi_{dc}[n_d] = n_d E_{dc}$ and E_{dc} is parametrized by the standard fully-localized-limit formula[5] $E_{dc} = U(n_d^0 - 1/2) - J/2(n_d^0 - 1)$, and n_d^0 is the nominal occupancy of the correlated ion. In particular, for the Ir^{4+} ion in Ruddlesden-Popper series we take $n_d^0 = 5$.

The DFT part of our code is based on the WIEN2k package.[6] The exchange-correlation energy in DFT ($\Phi_{xc}[\rho]$) is evaluated using the PBE functional.[7] The DFT+DMFT calculations are fully self-consistent in the electronic charge density, chemical potential, and impurity levels. The experimental crystal structures as obtained in Ref. 8, Ref. 9, and Ref. 10 are used for 214, 327, and 113, respectively. To obtain spectra on the real axis, maximum entropy method is used for analytical continuation of the self-energy.[11]

The energy range in computing the hybridizations and self-energies spanned a $20\,eV$ window around the Fermi energy (E_F), allowing us to use a set of system-independent local Coulomb interaction parameters U and J. This is in contrast to other DMFT calculations on iridates[19,20] where downfolding to Ir $t_{2g}-$orbitals was performed, so that the proper values of U and J depend sensitively on the screening by the bands eliminated from the model. The value of U for our large energy window was estimated for the undistorted 214 with tetragonal structure (P4/mmm) using the method of Ref. 14, which

leads to $U \approx 4.5\,\text{eV}$ and $J \approx 0.8\,\text{eV}$. To properly simulate the non-collinear magnetic state in 214, we chose different local coordinates on each Ir atom, with local quantization axis of spin in the direction of the ordered magnetic moment, and used proper Wigner rotations of spins and orbitals to transform the local self-energy to a common global axis.

The DOS and optical conductivities were computed from analytic continuation of the self-energy from the imaginary frequency axis to real frequencies using an auxiliary Green's function and the maximum-entropy method. The DMFT calculations were performed at 50 K, below the AFM transition temperature of the 214 (240 K)[15] and 327 (280 K)[16]. Brillouin zone integrations were done over 1000 k points in the whole zone in the self-consistent calculations and 8000 k points for the density of states and optical conductivity computations.

For comparison, we also carried out DFT+U calculations using the full-potential linearized augmented plane wave (FLAPW) method as implemented in the Elk code.[17] Since DFT+U does not include screening effects, the fully screened interaction on Ir is needed, which is here determined to be $U \approx 2.5\,\text{eV}$ by fitting the size of the gap and magnetic moments in 214 to the DMFT results. The calculations are done on a $4 \times 4 \times 1$ ($6 \times 6 \times 4$) k-mesh for the 214 and 327 (113) compounds with well converged total energies and magnetic moments.

When considering epitaxial strain, the out-of-plane lattice parameter and internal lattice coordinates are relaxed using VASP.[18] The plane-wave energy cutoff is taken to be 550 eV, with atomic forces converged to $1.0 \times 10^{-3}\,\text{eV/Å}$ in the GGA approximation. The calculations are done on a $6 \times 6 \times 2$ ($13 \times 13 \times 9$) k-mesh for the 214 and 327 (113) compounds. The magnitude of orbital and spin moments and their ratios calculated using VASP with GGA+U+SOC agree well with the values we presented using the Elk code.

II. VARIATION OF MAGNETIC MOMENTS WITH RESPECT TO EPITAXIAL STRAIN

The variation of the magnetic moments with respect to epitaxial strain can be understood utilizing the generalized effective $J=1/2$ wave functions defined in the main text (Eq. 1). Within the low-energy subspace of $\psi_{\pm 1/2}$, the orbital and spin moments can be evaluated by:

$$\langle \hat{O} \rangle = \begin{pmatrix} \langle \psi_{+1/2} \mid \hat{O} \mid \psi_{+1/2} \rangle & \langle \psi_{+1/2} \mid \hat{O} \mid \psi_{-1/2} \rangle \\ \langle \psi_{-1/2} \mid \hat{O} \mid \psi_{+1/2} \rangle & \langle \psi_{-1/2} \mid \hat{O} \mid \psi_{-1/2} \rangle \end{pmatrix},$$
(8)

where $\hat{O}$ is the spin/orbital moment operator S_α / L_α ($\alpha = x, y, z$), and $\psi_{\pm 1/2}$ refer to the generalized effec-

tive $J=1/2$ states

$$|\psi_{+\frac{1}{2}}\rangle = -\sqrt{\frac{3 - 2\gamma(\omega)^2}{3}}\, |d_{xy}\downarrow\rangle + \frac{\gamma(\omega)}{\sqrt{3}}(|d_{yz}\uparrow\rangle - i\,|d_{xz}\uparrow\rangle),$$

$$|\psi_{-\frac{1}{2}}\rangle = \sqrt{\frac{3 - 2\gamma(\omega)^2}{3}}\, |d_{xy}\uparrow\rangle + \frac{\gamma(\omega)}{\sqrt{3}}(|d_{yz}\downarrow\rangle + i\,|d_{xz}\downarrow\rangle),$$
(9)

defined in the main text.

Using these states, it is straightforward to derive the magnitude of the magnetic moments when magnetization points along z-direction:

$$\langle \mu_L^z \rangle = \frac{2}{3}\gamma^2 \Delta n \approx (\frac{2}{3} + \frac{4}{3}\tilde{\gamma})\Delta n$$
$$\langle \mu_S^z \rangle = (\frac{4}{3}\gamma^2 - 1)\Delta n \approx (\frac{1}{3} + \frac{8}{3}\tilde{\gamma})\Delta n,$$
(10)

and when it is in-plane:

$$\langle \mu_L^{xy} \rangle = \frac{2}{3}\gamma\sqrt{3 - 2\gamma^2}\Delta n \approx (\frac{2}{3} - \frac{2}{3}\tilde{\gamma})\Delta n$$
$$\langle \mu_S^{xy} \rangle = \frac{3 - 2\gamma^2}{3}\Delta n \approx (\frac{1}{3} - \frac{4}{3}\tilde{\gamma})\Delta n.$$
(11)

Here $\Delta n \equiv n_{1/2} - n_{-1/2}$ is the difference of the occupation numbers of the $\psi_{\pm 1/2}$ states.

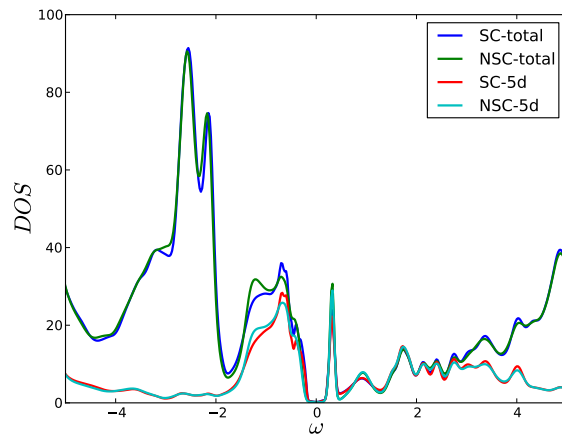## III. DENSITY OF STATES AND ORBITALLY RESOLVED SPECTRA

FIG. 1: Total Density of states and its $5d$ projection. SC corresponds to the fully charge self-consistent calculation, and NSC to the calculation with Kohn-Sham potentil fixed at the DFT charge.

In Fig. 1 we show the total Density of States (DOS) as well as orbitally resolved Ir-$5d$ DOS of Sr_2IrO_4 in an extended energy range. The oxygen states are peaked below $-2\,\text{eV}$ while the energy range between $-2\,\text{eV}$ and
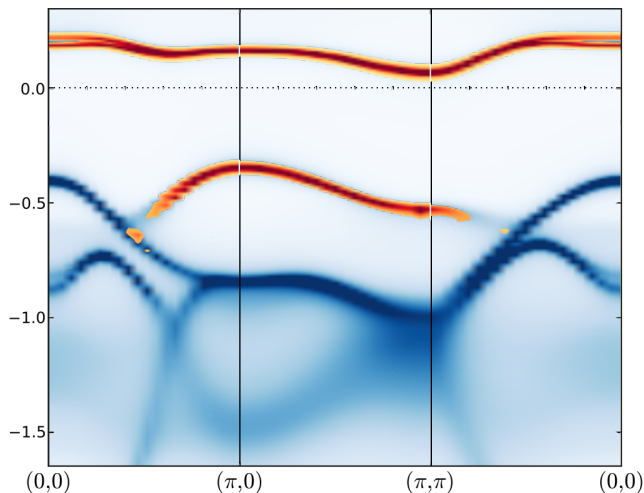
FIG. 2: Spectral function of Sr_2IrO_4 orbitally resolved into effective $J=1/2$ (orange) and $J=3/2$ (blue) components.

$+4\,\mathrm{eV}$ is dominated by Ir-5d states. A smaller part of the Ir-5d spectral weight is located at frequencies below

$-4\,\mathrm{eV}$.

Many implementations of LDA+DMFT do not update electronic charge on the self-consistent DMFT density matrix, instead in these implementations the LDA Kohn-Sham potential is fixed at the LDA charge density. We show in Fig. 1 that such non-charge self-consistent approximation to our functional Eq. (1) is a quite good approximation, since there is very little difference in the DOS in the two variants of the method. The main difference between our calculations and previous LDA+DMFT literature on Sr_2IrO_4[19,20] is then coming from the inclusion of oxygen ligands states, but not from charge self-consistency.

In Fig. 2 we resolve the momentum dependent spectral function of Sr_2IrO_4 into its orbital contributions from $J=1/2$ and $J=3/2$. As stated in the main text, the conduction band is overwhelmingly of $J=1/2$ nature, while the valence band has both $J=1/2$ and $J=3/2$ character. It is primarily of $J=1/2$ at $(\pi,0)$ point and of $J=3/2$ at $(0,0)$ point. Moreover, at $(0,0)$ point there is almost no weight with $J=1/2$ character in the occupied part of the spectra.

* corresp. author: hzhang@physics.rutgers.edu
[1] K. Haule, C.-H. Yee, and K. Kim, *Phys. Rev. B* **81**, 195107 (2010).
[2] G. Kotliar, S. Y. Savrasov, K. Haue, V. S. Oudovenko, O. Parcollet, and C. A. Marianetti, *Rev. Mod. Phys.* **78**, 865 (2006).
[3] K. Haule, *Phys. Rev. B* **75**, 155113 (2007).
[4] P. Werner, A. Comanac, L. de Medici, M. Troyer, and A. J. Millis, *Phys. Rev. Lett.* **97**, 076405 (2006).
[5] V. I. Anisimov, F. Aryasetiawan, and A. I. Lichtenstein, J. Phys.: Condens. Matter **9**, 767 (1997).
[6] P. Blaha, K. Schwarz, G. K. H. Madsen, K. Kvasnicka, and J. Luitz, in Wien2K, edited by K. Schwarz (Technische Universitat Wien), Austria, 2001.
[7] J.P. Perdew, K. Burke, and M. Ernzerhof, Phys. Rev. Lett. **77**, 3865 (1996).
[8] Q. Huang, J.L. Soubeyroux, O. Chmaissem, I.N. Sora, A. Santoro, R.J. Cava, J.J. Krajewski, and W.F. Peck, Jr., Journal of Solid State Chemistry **112**, 355 (1994).
[9] M.A. Subramanian, M.K. Crawford, and R.L. Harlow, Mater. Res. Bull. **29**, 645 (1994).
[10] J.G. Zhao, L.X. Yang, Y. Yu, F.Y. Li, R.C. Yu, Z. Fang, L.C. Chen, and C.Q. Jin, J. Appl. Phys. **103**, 103706 (2008).
[11] M. Jarrell, and J. E. Gubernatis, Physics Reports **269**, 133 (1996).
[12] R. Arita, J. Kunes, A.V. Kozhevnikov, A.G. Eguiluz, and M. Imada, Phys. Rev. Lett. **108**, 086403 (2012).
[13] C. Martins, M. Aichhorn, L. Vaugier, and S. Biermann, Phys. Rev. Lett. **107**, 266404 (2011).
[14] A. Kutepov, K. Haule, S.Y. Savrasov, and G. Kotliar, Phys. Rev. B **82**, 045105 (2010).
[15] G. Cao, J. Bolivar, S. McCall, J.E. Crow, and R.P. Guertin, Phys. Rev. B **57**, R11039 (1998).
[16] G. Cao, Y. Xin, C.S. Alexander, J.E. Crow, P. Schlottmann, M.K. Crawford, R.L. Harlow, and W. Marshall, Phys. Rev. B **66**, 214412 (2002).
[17] http://elk.sourceforge.net
[18] http://www.vasp.at
[19] R. Arita, J. Kunes, A.V. Kozhevnikov, A.G. Eguiluz, and M. Imada, Phys. Rev. Lett. **108**, 086403 (2012).
[20] C. Martins, M. Aichhorn, L. Vaugier, and S. Biermann, Phys. Rev. Lett. **107**, 266404 (2011).